Effects of α-cluster breaking on 3α-cluster structures in ^{12}C

Tadahiro Suhara

Matsue College of Technology, Matsue 690-8518, Japan

Yoshiko Kanada-En'yo

Department of Physics, Kyoto University, Kyoto 606-8502, Japan

To clarify the effects of α-cluster breaking on 3α-cluster structures in ^{12}C, we investigate ^{12}C using a hybrid model that combines the Brink-Bloch cluster model with the $p_{3/2}$ subshell closure wave function. We have found that α-cluster breaking caused by spin-orbit force significantly changes cluster structures of excited 0^+ states through orthogonality to lower states. Spatially developed cluster components of the 0_2^+ state are reduced. The 0_3^+ state changes from a vibration mode in the bending motion of three α clusters to a chainlike 3α structure having an open triangle configuration. As a result of these structure changes of 0^+ states, the band assignment for the 2_2^+ state is changed by the α-cluster breaking effect. Namely, in model calculations without the α-cluster breaking effect, the 0_2^+ state is assigned to be the band-head of the 2_2^+ state. However, when we incorporate α-cluster breaking caused by the spin-orbit force, the 0_3^+ state is regarded as the bandhead of the 2_2^+ state.

I. INTRODUCTION

In nuclear systems, an important feature is the independent single particle motion in a self-consistent mean field. As a result of spin-orbit splitting coming from the one-body spin-orbit potential, the jj-coupling shell model has been able to explain the nature of various nuclei. Another important feature is the development of clusters. Usually, well-developed cluster structures appear in excited states close to their cluster decay thresholds, as predicted by Ikeda's threshold rule [1].

In light nuclei, it is known that cluster formation occurs in low-lying states and competes with the shell-model structure. ^{12}C is a typical example of this competition [2–8]. Because the spin-orbit force usually tends to hinder the cluster formation, the ground state of ^{12}C is not the pure 3α-cluster state but is a mixture of 3α-cluster structure and jj-coupling shell model structure of the $p_{3/2}$ subshell closure; this is supported by the large level spacing between 0_1^+ and 2_1^+ states. On the other hand, in excited states of ^{12}C near the threshold energy, developed 3α-cluster structures have been discovered. It is important to understand the magnitude of this competition and how much it affects the structures of the ground and excited states of ^{12}C. To clarify this problem, it is necessary to have a theoretical model that can describe cluster structures incorporating cluster breaking effects. Nevertheless, many studies have investigated the cluster structures of ^{12}C using 3α-cluster models without considering cluster breaking. In the following, we review studies of structures of ^{12}C on the basis of various theoretical approaches and introduce recent developments in experimental works.

In 3α-cluster models, the ground and low-lying states have a compact triangle structure, whereas excited states near and above the 3α-cluster threshold energy have well-developed cluster structures [9–15]. For example, the 0_2^+ state, which is well known as the Hoyle state, is considered to be an α condensate state in which weakly interacting three α clusters occupy an identical lowest orbit of a mean-field potential [11–13]. This interpretation was indicated by the so-called

Tohsaki-Horiuchi-Schuck-Röpke (THSR) wave function. The cluster developed structure in the 0_2^+ state is also experimentally supported by a quite large monopole transition strength [16]. Another interesting cluster structure was predicted in the 0_3^+ state, which is considered to be a vibration mode of acute and obtuse triangle configurations [9]. However, 3α-cluster models cannot describe the detailed properties of ground and excited states of ^{12}C because they ignore the components of α-cluster breaking caused by the spin-orbit force. For example, the excitation energy of the 2_1^+ state is underestimated.

In the no-core shell model calculation, which is one of the *ab initio* calculations, many states of ^{12}C are reproduced well [17,18]. However, the model fails to reproduce some states observed near the cluster threshold such as 0_2^+ and 0_3^+ states. This seems to be reasonable because these states are cluster developed states in which a large proportion of nucleons are distributed over many harmonic oscillator orbits. To describe these cluster developed states, a model space is required that is significantly larger than those used in the usual no-core shell model calculation [19].

Another *ab initio* calculation for ^{12}C has been performed using the chiral effective field theory [20]. However, quantitative reproduction of structure properties, such as radii, was not satisfactory even though the calculation reproduced some experimental data such as excitation energies and $E2$ transition strengths. For detailed discussion of cluster structures, further developments are required.

The antisymmetrized molecular dynamics (AMD) and the fermionic molecular dynamics (FMD) models have been successful in describing the nature of ^{12}C from the ground state to the higher excited states [2–7]. In these models, the ground and low-lying states are a mixture of cluster and jj-coupling shell model configurations. Because of this mixing, these models reproduce well the excitation energy of the 2_1^+ state and $E2$ transition strengths between the low-lying states. For states near the threshold, these models reproduce the cluster nature, but the detailed cluster structures

obtained with these models are somewhat different from those of cluster model results. For example, the radius of the 0_2^+ state can be somewhat smaller than that predicted by the cluster model, although both models reproduce the monopole transition strength [21]. The 0_3^+ state is considered to be a chainlike structure having an obtuse triangle configuration of three α clusters instead of the vibrational state predicted by the cluster model. The capability of reproducing the experimental data of ^{12}C is a significant advantage of AMD and FMD.

Recently, several interesting experimental data on ^{12}C for excited states near the threshold energy have been reported. A new state, the 2_2^+ state at 9.84 MeV, was discovered [22–24]. The $B(E2)$ transition strength from this 2_2^+ state to the ground state was measured to be $1.57^{+0.14}_{-0.11}e^2$ fm^4 [25], which many models fail to reproduce. Itoh *et al.* found that the broad 0^+ state at 10 MeV consists of two 0^+ states [26]. Theoretically, the existence of two 0^+ states above the 0_2^+ state was predicted by Kurokawa and Katō [27,28] and also shown by Ohtsubo *et al.* [29] using the orthogonal condition model and the complex scaling method (OCM+CSM). A band structure including these new states has been an open problem. In particular, the assignment of the band-head state of the newly measured 2_2^+ state is now controversial.

In this paper, we investigate ^{12}C with a simple model to clarify α-cluster breaking effects on 3α-cluster structures. In this model, we superpose the Brink-Bloch (BB) cluster model wave functions and the $p_{3/2}$ subshell closure wave function to incorporate the mixing of cluster breaking components in cluster structures. This model is regarded as an extension of the generator coordinate method of a cluster model. The difference from traditional cluster models is the mixing of the $p_{3/2}$ subshell closure wave function, which is the lowest configuration of the jj-coupling shell model. The results obtained with this model are consistent with the AMD and FMD results even though it is much simpler than those models. In this model space, we changed the strength of the spin-orbit force by hand to control the mixing of the α-cluster breaking component, i.e., the $p_{3/2}$ subshell closure wave function. We found that the mixing of the α-cluster breaking component significantly changes the cluster configurations and band structure of excited states.

This paper is organized as follows. In Sec. II, we explain the wave function and Hamiltonian used in the present study. In Sec. III, we show calculated results. In Sec. IV, we discuss differences in cluster configurations in 0^+ states and band structure between calculations with and without α-cluster breaking. We compare our results with other theoretical calculations. Finally, we summarize the findings of the present study in Sec. V.

II. FORMULATION

A. Wave function

In this work, we investigate ^{12}C using a simple model that combines the BB cluster model with the lowest wave function of the jj-coupling shell model. We superpose many 3α BB wave functions and the single $p_{3/2}$ subshell closure wave function.
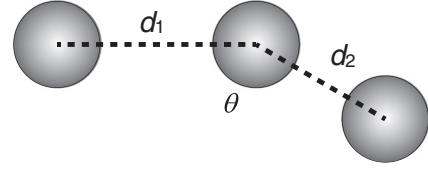

FIG. 1. Schematic of a 3α-cluster structure. The configuration is characterized by the distances between α clusters, d_1 and d_2, and the bending angle θ.

The BB wave function [30] for three α clusters is written as

$$\Phi^{(\mathrm{BB})}(\boldsymbol{R}_1, \boldsymbol{R}_2, \boldsymbol{R}_3) = \mathcal{A}\left[\varphi_1^\alpha, \varphi_2^\alpha, \varphi_3^\alpha\right], \tag{1}$$

$$\varphi_i^\alpha = \phi_{\boldsymbol{R}_i}\phi_{\boldsymbol{R}_i}\phi_{\boldsymbol{R}_i}\phi_{\boldsymbol{R}_i}\chi_{p\uparrow}\chi_{p\downarrow}\chi_{n\uparrow}\chi_{n\downarrow}, \tag{2}$$

$$\phi_{\boldsymbol{R}_i} = \left(\frac{2\nu}{\pi}\right)^{3/4}\exp[-\nu(\boldsymbol{r} - \boldsymbol{R}_i)^2], \tag{3}$$

where $\boldsymbol{R}_i$ is a real vector that indicates the position of the ith α cluster. For the width parameter, we use the value $\nu = 0.235$ fm^{-2}, the same as that used in the previous study of ^{12}C using AMD [21]. This parameter was originally from a variational calculation for the ground state of ^{9}Be in Ref. [31]. The configuration of the BB wave function is characterized by the distances between α clusters, d_1 and d_2, and the bending angle θ, as shown in Fig. 1. Because of symmetry, we can limit distances to $d_1 \leqslant d_2$ without loss of generality. To describe relative motions of clusters sufficiently, we generate 252 BB wave functions by taking the distance $d_i = 1, 2, \ldots, 6$ fm and the bending angle $\theta = n\pi/12$ with $n = 1, 2, \ldots, 12$.

To describe the $p_{3/2}$ subshell closure wave function, we adopted the method proposed in Refs. [32,33]. In this method, the single particle wave function is described by a Gaussian wave packet in the same manner as in the BB wave function Eq. (3). However, the center of the wave packet for the jth nucleon belonging to the ith α cluster is replaced by a complex parameter $\boldsymbol{\zeta}_j$,

$$\boldsymbol{\zeta}_j = \boldsymbol{R}_i + i e_j^{\mathrm{spin}} \times \boldsymbol{R}_i, \tag{4}$$

where e_j^{spin} is a unit vector for the intrinsic spin direction of the jth nucleon. In the limit of $\boldsymbol{R}_i \to 0$, this wave function describes the $p_{3/2}$ subshell closure wave function. For the width parameter of the $p_{3/2}$ subshell closure wave function, we use the same value $\nu = 0.235$ fm^{-2} of the BB wave function to exactly separate the center-of-mass motion from the total wave function.

As the final wave function, we superpose the 252 3α BB wave functions and the single $p_{3/2}$ subshell closure wave function with the parity and angular momentum projection,

$$|\Psi_{J^\pi}\rangle = \sum_{i,K} c_{iK}^{J^\pi} \hat{P}_{MK}^{J^\pi} |\Phi_i^{(\mathrm{BB})}\rangle + c_{p_{3/2}} \hat{P}_{MK}^{J^\pi} |p_{3/2}\rangle, \tag{5}$$

where $\hat{P}_{MK}^{J^\pi}$ is the parity and angular momentum projection operator. The coefficients are determined by the diagonalization of the norm and Hamiltonian matrices.

The superposition of BB wave functions without the $p_{3/2}$ subshell closure wave function corresponds to the traditional 3α-cluster GCM calculation without α-cluster breaking. In the present model, α-cluster breaking caused by the spin-orbit force is incorporated by adding the $p_{3/2}$ subshell closure wave function to the 3α-cluster model space. Note that the final wave functions for the nonzero angular momentum states are the same as those obtained by the 3α-cluster GCM calculation because the single $p_{3/2}$ subshell closure wave function is a $J^{\pi} = 0^+$ eigenstate; therefore, $\hat{P}^{J^{\pi}}_{MK}|p_{3/2}\rangle$ vanishes for $J^{\pi} \neq 0^+$. In other words, the α-cluster breaking caused by the spin-orbit force affects only the 0^+ states through the mixing of the $p_{3/2}$ subshell closure wave function.

In the present work, we omit cluster breaking components for the $J^{\pi} \neq 0^+$ states because they give only minor effect compared with the significant cluster breaking effects in the $J^{\pi} = 0^+$ states. Indeed, the structure of the cluster developed states does not change qualitatively even if we adopt the cluster breaking components for the $J^{\pi} \neq 0^+$ states. To simplify the discussion, we adopt only the $p_{3/2}$ subshell closure wave function, which gives the major contribution of the α-cluster breaking effect.

B. Hamiltonian

The Hamiltonian consists of the kinetic energy $\hat{t}_i$, effective central force $\hat{V}^{\text{cent.}}_{ij}$, effective spin-orbit force $\hat{V}^{\text{LS}}_{ij}$, and Coulomb force $\hat{V}^{\text{Coul.}}_{ij}$,

$$\hat{H} = \sum_i \hat{t}_i - \hat{T}_G + \sum_{i<j} \hat{V}^{\text{cent.}}_{ij} + \sum_{i<j} \hat{V}^{\text{LS}}_{ij} + \sum_{i<j} \hat{V}^{\text{Coul.}}_{ij}, \quad (6)$$

where the center-of-mass kinetic energy $\hat{T}_G$ is subtracted. For the effective central force, we used the Volkov No. 2 force [34] with Majorana parameter $M = 0.60$. For the effective spin-orbit force, we used the spin-orbit term of the G3RS interaction [35],

$$\hat{V}^{\text{LS}}_{ij} = \sum_{k=1}^{2} u_k \exp\left[-\left(\frac{\hat{r}_{ij}}{b_k}\right)^2\right] \hat{P}(^3O)\hat{\boldsymbol{L}} \cdot \hat{\boldsymbol{S}}, \quad (7)$$

where $\hat{P}(^3O)$ is a projection operator onto the triplet odd state. We chose $u_1 = -u_2 \equiv u_{\text{ls}}$, where u_{ls} is the strength of the spin-orbit force. We used the same interaction with $u_{\text{ls}} = 1600$ MeV as that used in a previous study of ^{12}C using AMD [21]. We also investigate the u_{ls} dependence of energy levels and the degree of α-cluster breaking by changing the strength u_{ls} from 0 to 3200 MeV.

III. RESULTS

In Fig. 2, we show the energy levels of 0^+ and 2^+ states calculated with the present model using $u_{\text{ls}} = 1600$ MeV, which is the same strength used in our previous study of ^{12}C using AMD [21], and those obtained with the 3α-cluster GCM calculation. The former and the latter correspond to calculations with and without α-cluster breaking, i.e., the mixing of the $p_{3/2}$ subshell closure wave function caused by the spin-orbit force, which we call "$3\alpha + p_{3/2}$" and "3α," respectively. Experimental data are taken from Refs. [23,26,36].
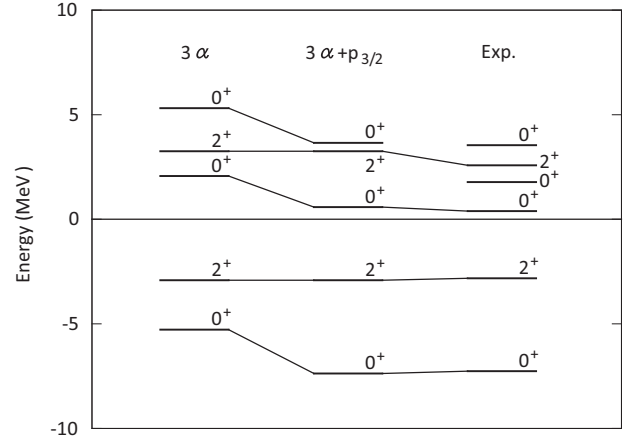

FIG. 2. Comparison of calculated energy levels of 0^+ and 2^+ states with experimental ones. Energies are measured from the 3α threshold energy. Theoretical and experimental threshold energies are -82.9 and -84.9 MeV, respectively. Levels labeled as "3α" and "$3\alpha + p_{3/2}$" show cluster model results and present results for $u_{\text{ls}} = 1600$ MeV, respectively.

Energies are measured from the 3α threshold energy. The theoretical and experimental threshold energies are -82.9 and -84.9 MeV, respectively.

In the 3α case, the spin-orbit force provides zero energy contribution because the expectation value of the spin-orbit force vanishes in the pure 3α-cluster model space. In the $3\alpha + p_{3/2}$ result, the 2^+ states are completely the same as those of the 3α result, but the 0^+ energies are decreased by the spin-orbit force because of the mixing of the $p_{3/2}$ subshell closure wave function. The results for $3\alpha + p_{3/2}$ agree with experimental results very well except for the absence of a 0^+ state observed around 10 MeV. In particular, the level spacing between 0_1^+ and 2_1^+ states of $3\alpha + p_{3/2}$ agrees well with the experimental one, which is largely underestimated in 3α. This large spacing comes from the energy gain of the spin-orbit force in the 0_1^+ state with the mixing of the $p_{3/2}$ subshell closure wave function. Any microscopic α-cluster model fails to reproduce this large level spacing, and therefore, this is an evidence for α-cluster breaking.

As shown later, the $3\alpha + p_{3/2}$ result is qualitatively consistent with the AMD and FMD results for ^{12}C. This implies that the major difference between the AMD and FMD results and 3α-cluster model calculations is the α-cluster breaking effect, which can be qualitatively simulated by the mixing of only one configuration of the $p_{3/2}$ subshell closure to the 3α-cluster model space in the present model. In Sec. IV, we discuss in detail the structure differences between 0^+ states with and without α-cluster breaking.

As mentioned above, α-cluster breaking caused by the spin-orbit force gives a significant effect in ^{12}C. To clarify the mechanism of the mixing of the α-cluster breaking component, we consider the dependence of 0^+ states on the strength of the spin-orbit force by changing the strength parameter u_{ls} from 0 to 3200 MeV in the present model. The calculation using $u_{\text{ls}} = 0$ MeV is equivalent to the 3α calculation. As the strength of the spin-orbit force increases, 0^+ energy levels
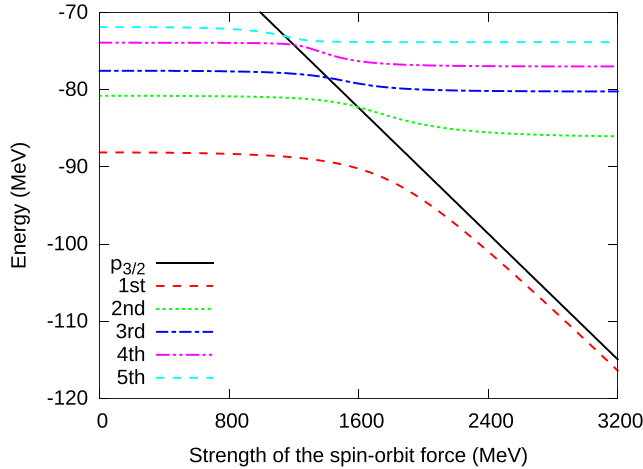
FIG. 3. (Color online) Change in energy levels of 0^+ states against the strength of the spin-orbit force u_{ls}. Solid line is the energy of the $p_{3/2}$ subshell closure wave function.

change due to α-cluster breaking, i.e., the $p_{3/2}$ subshell closure wave function.

In Fig. 3, we show the change in energy levels of 0^+ states against the strength of the spin-orbit force u_{ls}. The energy of the $p_{3/2}$ subshell closure wave function is also shown for reference. For $u_{ls} \leqslant 800$ MeV, the energies are almost independent of the strength of the spin-orbit force. In this region, the energy levels and wave functions themselves are almost equal to those obtained from the pure cluster model calculation without α-cluster breaking. When $u_{ls} \geqslant 2400$ MeV, the 0^+ levels except for the lowest one do not depend on the strength of the spin-orbit force; however, the energy of the lowest 0^+ state linearly decreases and shows almost the same u_{ls} dependence as that of the $p_{3/2}$ subshell closure state. These imply that structures of the states do not change when the strength of the spin-orbit force is extremely weak or strong. However, around $u_{ls} = 1600$ MeV, energy levels depend on the strength u_{ls} because of level crossings of the cluster states and the $p_{3/2}$ subshell closure wave function. In this transient region, a change in the wave function occurs for each state.

In Table I, we show the squared overlaps between the 0^+ GCM wave functions and the $p_{3/2}$ subshell closure wave

TABLE I. Percentages of squared overlaps between 0^+ GCM wave functions and the $p_{3/2}$ subshell closure wave function for $u_{ls} = 0, 800, 1600, 2400, 3200$ MeV.

State	u_{ls} (MeV)				
	0	800	1600	2400	3200
0_1^+	2.46	6.11	34.3	89.6	97.0
0_2^+	0.51	1.86	25.9	6.08	1.14
0_3^+	0.43	1.96	16.8	1.13	0.25
0_4^+	0.07	0.54	14.0	0.93	0.25
0_5^+	0.68	5.82	0.71	0.25	0.02

TABLE II. Rms radii of 0^+ states. Experimental data are from Refs. [37,38]. The unit is fm.

State	u_{ls} (MeV)					Expt.
	0	800	1600	2400	3200	
0_1^+	2.53	2.51	2.35	2.11	2.09	2.35 ± 0.02
0_2^+	3.44	3.43	2.99	2.70	2.69	2.89 ± 0.04
0_3^+	3.63	3.62	3.39	3.50	3.51	
0_4^+	3.76	3.74	3.40	3.60	3.62	
0_5^+	3.76	3.74	3.83	3.81	3.81	

function,

$$O_{p_{3/2}} = |\langle \Psi_{0^+} | p_{3/2} \rangle|^2, \qquad (8)$$

for $u_{ls} = 0, 800, 1600, 2400, 3200$ MeV. These overlaps measure the magnitude of α-cluster breaking. For $u_{ls} \leqslant 800$ MeV, there is little, if any, α-cluster breaking in 0^+ states. In particular, for $u_{ls} = 0$ MeV, 0^+ states are composed of pure 3α-cluster components decoupled from the α-clusters breaking component. Note that the $p_{3/2}$ subshell closure wave function is not orthogonal to the 3α-cluster wave functions but slightly overlaps with the 0^+ projected SU(3)-limit 3α-cluster wave function,

$$\left| \langle p_{3/2} | \hat{P}_{00}^{0^+} | SU(3) \rangle \right|^2 = 5/81. \qquad (9)$$

Therefore, even for $u_{ls} = 0$ MeV without α-cluster breaking, the squared overlap of the 0_1^+ state is not zero but finite of the same order as 5/81. For $u_{ls} \geqslant 2400$ MeV, the 0_1^+ state is dominated by the $p_{3/2}$ subshell closure wave function. This implies that α clusters are broken almost completely in the lowest state. For higher states, there is no α-cluster breaking. For $u_{ls} = 1600$ MeV, the squared overlaps for $0_{1,2,3,4}^+$ states are 10–30%, which implies that significant components of α clusters are broken in these states. In other words, 3α-cluster states couple significantly with the cluster breaking configuration in these states.

In Table II, we show the root-mean-square (rms) radii of the 0^+ states for $u_{ls} = 0, 800, 1600, 2400, 3200$ MeV. Reproduction of experimental values is fairly good at $u_{ls} = 1600$ MeV. As the strength of the spin-orbit force increases, the radii of the 0_1^+ and 0_2^+ states decrease. The shrinking mechanism differs between 0_1^+ and 0_2^+ states. For the 0_1^+ state, the shrinking comes from the decreasing of 3α-cluster components by the significant mixing of the $p_{3/2}$ subshell closure wave function. However, for the 0_2^+ state, this decrease mainly comes from the mixing of relatively compact cluster components because of orthogonality to the 0_1^+ state. As the strength of the spin-orbit force increases, the 3α component decreases in the 0_1^+ state, which makes the 0_2^+ state include more compact 3α-cluster components. Details are discussed in Sec. IV.

In Table III, we show the monopole transition strengths between 0^+ states. The transition strengths rapidly change around $u_{ls} = 1600$ MeV. The $0_1^+ \rightarrow 0_2^+$ transition strength for the strong spin-orbit force is smaller than that for the weak spin-orbit force. This result is consistent with the fact that the 0_1^+ state becomes dominated by the $p_{3/2}$ subshell closure wave

TABLE III. Monopole transition strengths between 0^+ states. Experimental data are from Ref. [36]. The unit is fm^2.

Transition	u_{ls} (MeV)					Expt.
	0	800	1600	2400	3200	
$0_1^+ \to 0_2^+$	8.2	8.1	8.1	2.8	1.3	5.4 ± 0.2
$0_1^+ \to 0_3^+$	5.5	5.4	2.1	0.5	0.4	
$0_2^+ \to 0_3^+$	10.7	10.9	16.8	10.6	9.7	

function and loses the cluster correlation, which enhances the monopole transition strength to the cluster developed states.

The mixing of the α-cluster breaking in 0^+ states also affects the $E2$ transition strengths between 0^+ and 2^+ states. The calculated $E2$ transition strengths from 2^+ states to 0^+ states are shown in Table IV. Similar to the monopole transition strengths, the $E2$ transition strengths change drastically around $u_{ls} = 1600$ MeV. The agreement between theoretical and experimental results is rather good around $u_{ls} = 1600$ MeV, but it is worse in both the strong and weak limits of the strength of spin-orbit force. Considering the overall results presented up to here, reproduction of experimental values is better around $u_{ls} = 1600$ MeV, where the degree of mixing of cluster and cluster breaking components is significant not only in the ground state but also in excited 0^+ states.

The $E2$ transition strengths from the 2_2^+ state are important for determining the band assignment for this state, which has been attracting significant interest. Its $E2$ transition strengths to the $0_{2,3}^+$ states are remarkably large. Interestingly, the behavior of the magnitude is reversed by α-cluster breaking in the change from $u_{ls} = 800$ to 1600 MeV. For $u_{ls} = 0$ MeV in the weak limit of the spin-orbit force, the $2_2^+ \to 0_2^+$ transition strength is almost three times larger than the $2_2^+ \to 0_3^+$ one. However, for $u_{ls} = 1600$ MeV, the $2_2^+ \to 0_3^+$ transition strength is larger by a factor of 2 than the $2_2^+ \to 0_2^+$ one. The strongest $E2$ transition to the 0_3^+ state for $u_{ls} = 1600$ MeV, in which the reproduction of experimental results is good, indicates that the 0_3^+ state is likely to be the bandhead of the 2_2^+ instead of the 0_2^+ state.

The present results indicate that the band structure of higher excited states is affected by α-cluster breaking caused by the spin-orbit force. Even though the $0_{2,3}^+$ states for $u_{ls} = 1600$ MeV still contain dominant 3α-cluster configurations, their $E2$ transition strengths from the 2_2^+ state are

TABLE IV. $E2$ transition strengths from 2^+ states to 0^+ states. Experimental data are from Refs. [25,36]. The unit is $e^2\,fm^4$.

Transition	u_{ls} (MeV)					Expt.
	0	800	1600	2400	3200	
$2_1^+ \to 0_1^+$	10.8	10.6	7.4	1.2	0.4	7.6 ± 0.4
$2_1^+ \to 0_2^+$	1.4	1.6	5.1	11.1	11.8	2.6 ± 0.4
$2_1^+ \to 0_3^+$	0.4	0.4	0.2	0.2	0.3	
$2_2^+ \to 0_1^+$	4.0	3.6	1.1	0.0	0.0	$1.57^{+0.14}_{-0.11}$
$2_2^+ \to 0_2^+$	183	179	76.5	14.8	12.0	
$2_2^+ \to 0_3^+$	64.4	69.8	166	206	207	

considerably different from those with $u_{ls} = 0$ and 800 MeV for the calculation without α-cluster breaking. The critical effect of α-cluster breaking on the 2_2^+ band assignment mainly originates from the change of 3α configurations in the cluster model space. More details of the cluster structure change of the 0_2^+ and 0_3^+ states caused by α-cluster breaking are discussed in the next section.

IV. DISCUSSION

A. Structure changes of 0^+ states

To investigate the structure changes of 0^+ states by α-cluster breaking, we focus on 3α configurations contained in 0^+ states obtained from calculations with and without α-cluster breaking. We show the energy surface for 3α configurations in Fig. 4. The figure shows the 0^+ energy of a single BB wave function for the isosceles triangle configuration (equal distances, $d_1 = d_2 \equiv d$) on the two-dimensional plane for distance and angle. Note that the spin-orbit force has no energy contribution in the 3α subspace.

Around $(d,\theta) = (2.5 \text{ fm}, 60°)$, a rather deep minimum exists, which corresponds to the ground state of ^{12}C in the pure 3α model space. The 3α-cluster structure in this region with finite distances has an equilateral triangle shape and has a spatial development to some extent. This indicates that higher cluster correlation beyond the SU(3) shell model limit is contained even in the ground state. Around $(d,\theta) = (4.0 \text{ fm}, 130°)$ for obtuse (open) triangle structures, a plateau with an energy of -74 MeV exists and continues into the area of small bending angles for acute triangle structures. In the 3α-cluster model calculation without α-cluster breaking, α clusters move almost freely on this soft mode of energy surface involving various triangle configuration, and construct the 0_2^+ state, which is a typical example of "gaslike" cluster states. The 0_3^+ state as the vibrational excitation is built on top of the 0_2^+ state along this soft energy surface, as suggested by Uegaki *et al.* [9]. This situation changes somewhat when α-cluster breaking occurs.
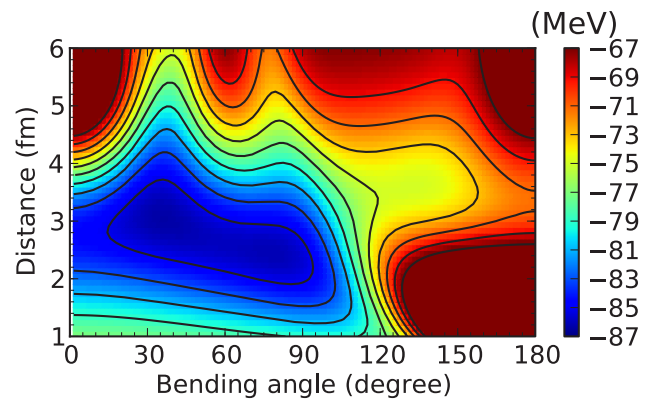

FIG. 4. (Color online) 0^+ energy surface of a single BB wave function for 3α clusters in which equal distances between α clusters are assumed, i.e., $d_1 = d_2 \equiv d$.
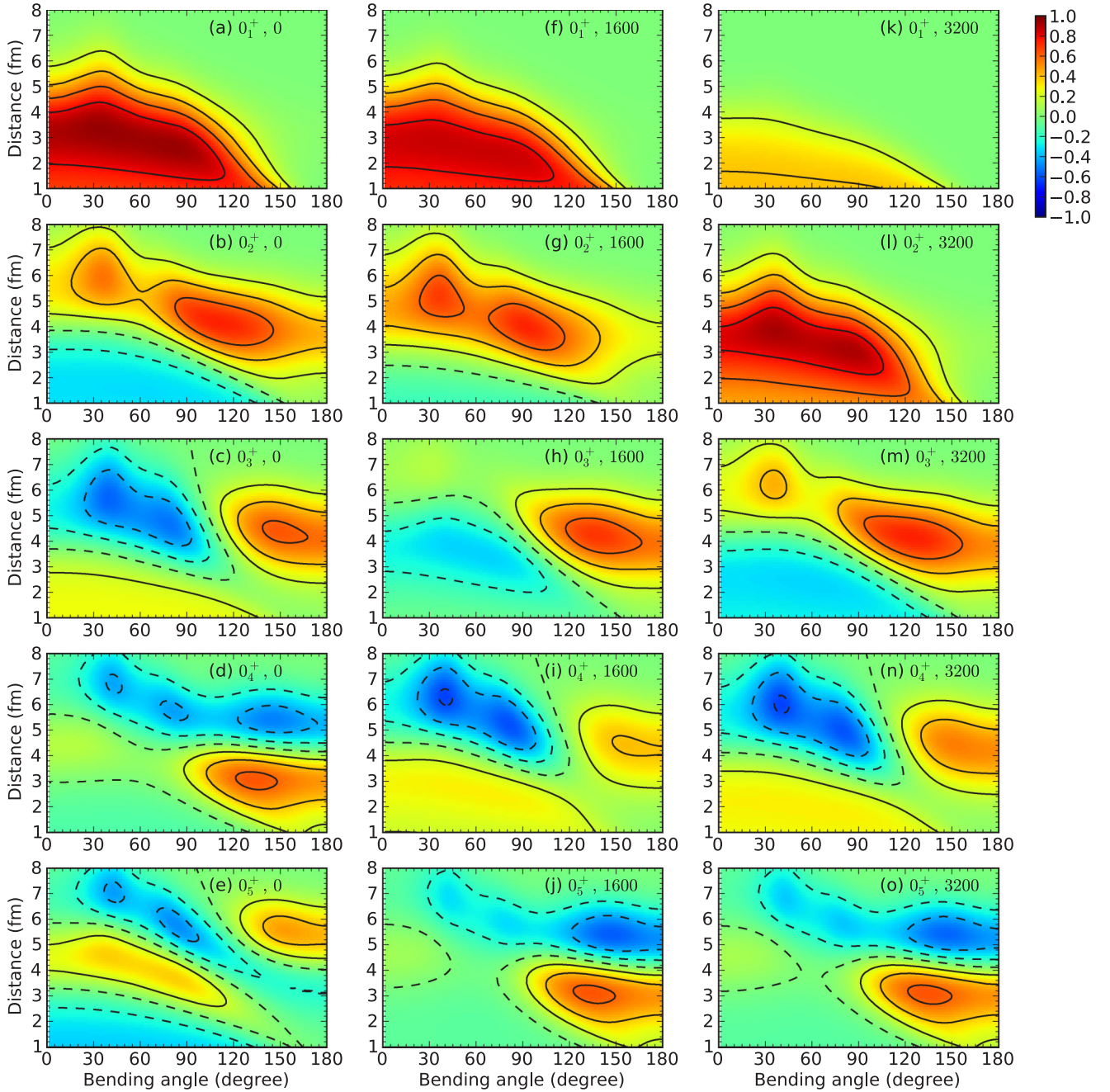
FIG. 5. (Color online) Overlap surfaces between 0^+ GCM states and single BB wave functions for $u_{ls} = 0$, 1600, 3200 MeV are shown in left, middle, and right columns, respectively. For the BB wave function, the isosceles triangle structure, $d_1 = d_2 \equiv d$, is assumed.

In Fig. 5, we show overlap surfaces between the 0^+ GCM states for $u_{ls} = 0$, 1600, 3200 MeV and the single BB wave functions,

$$O(d,\theta) = \langle \Psi_{0^+} | \Phi^{(\mathrm{BB})}(d,\theta) \rangle. \qquad (10)$$

For the BB wave function, the isosceles triangle structure is assumed. These overlap surfaces show the cluster motion projected onto the 3α-cluster configuration space for 0^+ states. The $u_{ls} = 0$ MeV result for the weak limit of the spin-orbit force corresponds to the 3α-cluster model calculation without α-clusters breaking. The $u_{ls} = 3200$ MeV result for the strong limit of the spin-orbit force is the extreme case in which the

$p_{3/2}$ subshell closure state comes down to the lowest state after level crossing over 3α-cluster states is completed, as described in the previous section. The $u_{ls} = 1600$-MeV result reproduces well the experimental results, as explained above, and is considered to be a reasonable result with the mixing of α-cluster breaking. We discuss how α-cluster breaking affects cluster structures in 0^+ states by comparing the results with and without α-cluster breaking, corresponding to $u_{ls} = 0$ MeV and $u_{ls} = 1600$ MeV, respectively.

First we compare the structure of the 0_1^+ state with and without α-cluster breaking. For $u_{ls} = 0$ MeV (without α-cluster breaking), the wave function has a large overlap

around the energy minimum in the 3α-cluster model space and also contains components of developed cluster configurations with larger intercluster distances than the energy minimum configuration. For $u_{ls} = 1600$ MeV (with α-cluster breaking), the behavior of the overlap surface is similar to that for $u_{ls} = 0$ MeV. However, the absolute amplitude around the energy minimum decreases and 3α-cluster components become small because of the significant mixing of the $p_{3/2}$ subshell closure component in the $0_1{}^+$ state, as shown in Table I.

Next we discuss α-cluster breaking effects on the structure of the $0_2{}^+$ state, which reflects the structure change of the $0_1{}^+$ state because of the orthogonal condition to lower states. For $u_{ls} = 0$ MeV (without α-cluster breaking), the overlap is distributed over a wide area of well-developed cluster structures, indicating that the $0_2{}^+$ state is described by the superposition of various triangle configurations of three α clusters. Consequently, it has a large rms radius, as explained above. For $u_{ls} = 1600$ MeV (with α-cluster breaking), the overlap is also distributed over a wide area of well-developed cluster structures and is qualitatively similar to the distribution for $u_{ls} = 0$ MeV. However, quantitatively, the overlap shifts to smaller bending angles and the components for acute triangles are slightly enhanced. Moreover, the maximum peaks also shift toward a shorter distances region compared to those for $u_{ls} = 0$ MeV.

These results imply that the spatial development of the cluster structure is reduced in the $0_2{}^+$ state. Namely, the gaslike feature of the $0_2{}^+$ state is slightly reduced by α-cluster breaking, implying that α-cluster breaking has the effect of attracting α clusters. The differences in cluster structures in the $0_2{}^+$ states for $u_{ls} = 1600$ MeV and for $u_{ls} = 0$ MeV can be understood as follows. Without α-cluster breaking, the compact 3α-cluster component in the $0_2{}^+$ is hindered due to orthogonality to the $0_1{}^+$ state, which has a compact 3α-cluster structure. With α-cluster breaking, this hindrance is weakened because the 3α-cluster component in the $0_1{}^+$ state decreases with the mixing of the noncluster component of the $p_{3/2}$ subshell closure configuration.

In the structure of the $0_3{}^+$ state, a qualitative difference is observed between the results with and without α-cluster breaking. For $u_{ls} = 0$ MeV (without α-cluster breaking), the phase of the overlap changes as θ increases along the line for $d \sim 5$ fm. It has a negative minimum around $(d,\theta) = (5.5$ fm, $60°)$ and a positive maximum $(d,\theta) = (4$ fm, $150°)$ with almost the same amplitude. This indicates that the $0_3{}^+$ state is the vibration mode of acute and obtuse triangle configurations. For $u_{ls} = 1600$ MeV (with α-cluster breaking), the behavior differs from the vibration mode. The amplitude of the negative minimum for the acute triangle configuration is considerably hindered, and as a result, the $0_3{}^+$ state is dominated by the obtuse triangle configuration.

The hindrance in the amplitude around $\theta = 60°$ originates from orthogonality to the $0_2{}^+$ state. As explained above, the components of acute triangle configurations increase in the $0_2{}^+$ state; therefore, the $0_3{}^+$ state loses components of acute triangle configurations due to orthogonality to the $0_2{}^+$ state. The components of obtuse triangle configurations in the $0_2{}^+$ state are relatively smaller than those of acute triangle configurations, and as a result, the overlap for the $0_3{}^+$ state
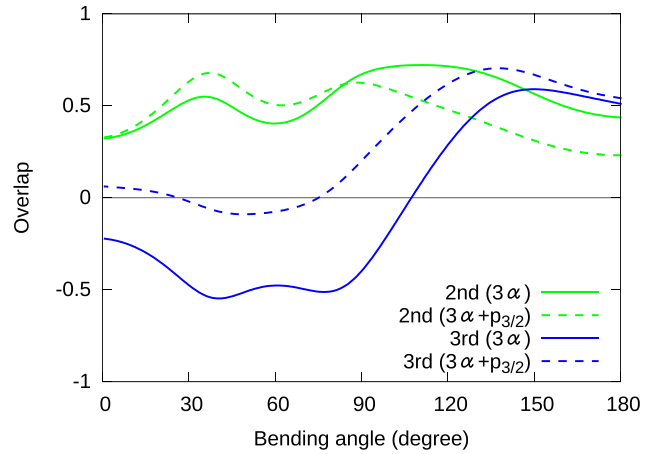

FIG. 6. (Color online) Overlap curves between 0^+ GCM states and single BB wave functions for $u_{ls} = 0$ MeV (3α) and $u_{ls} = 1600$ MeV (3$\alpha + p_{3/2}$) on the $d = 6.0 - 2.5\theta/180°$ line.

concentrates on obtuse triangle configurations for a chain-like open triangle structure. Because of α-cluster breaking, the structure of the $0_3{}^+$ state changes from the vibration mode of acute and obtuse triangle configurations to the chainlike open triangle structure. Hence, α-cluster breaking produces significant effects not only in the ground state but also in the cluster configurations of excited states. This is surprising because the naive expectation is that α-cluster breaking can affect only ground state properties.

To compare in more detail the results with and without α-cluster breaking for the $0_2{}^+$ and $0_3{}^+$ states, Fig. 6 shows a one-dimensional plot of the overlap of 0^+ GCM states for $u_{ls} = 0$ MeV (3α) and $u_{ls} = 1600$ MeV (3$\alpha + p_{3/2}$) with the single BB wave functions on the $d = 6.0 - 2.5\theta/180°$ line. In the 3α case, the overlap curve for the $0_2{}^+$ state is distributed almost uniformly over the entire region of the bending angle θ. To satisfy the orthogonal condition to the $0_2{}^+$ state, the overlap curve of the $0_3{}^+$ has a nodal structure with a node at $\theta = 100°$ and almost the same heights of negative and positive amplitudes. In the 3$\alpha + p_{3/2}$ case, the overlap curve of the $0_2{}^+$ state leans toward the small θ region. The overlap curve of the $0_3{}^+$ leans toward the large θ region, where chainlike open triangle configurations of three α clusters appear.

The $u_{ls} = 3200$-MeV result for the strong limit of the spin-orbit force is the extreme case in which the $p_{3/2}$ subshell closure state comes down to the lowest state after the level crossing over 3α-cluster states is completed. Because the model space of 3α-cluster configurations almost decouples from the $p_{3/2}$ subshell closure wave function in the ground state, 3α-cluster structures appear in excited 0^+ states. Consequently, the $0_2{}^+$, $0_3{}^+$, and 0_4^+ have 3α-cluster structures of the compact triangle, gaslike, and vibrational states; these are qualitatively similar to those of the $0_1{}^+$, $0_2{}^+$, and $0_3{}^+$ states in the $u_{ls} = 0$ MeV results obtained without α-cluster breaking, respectively. Strictly, the $p_{3/2}$ subshell closure wave function is not orthogonal to the 3α-cluster model space, and its component in the ground state partially truncates the 3α-cluster model space; therefore, the consistency of cluster structures between $u_{ls} = 0$ MeV and $u_{ls} = 3200$ MeV is not entire.
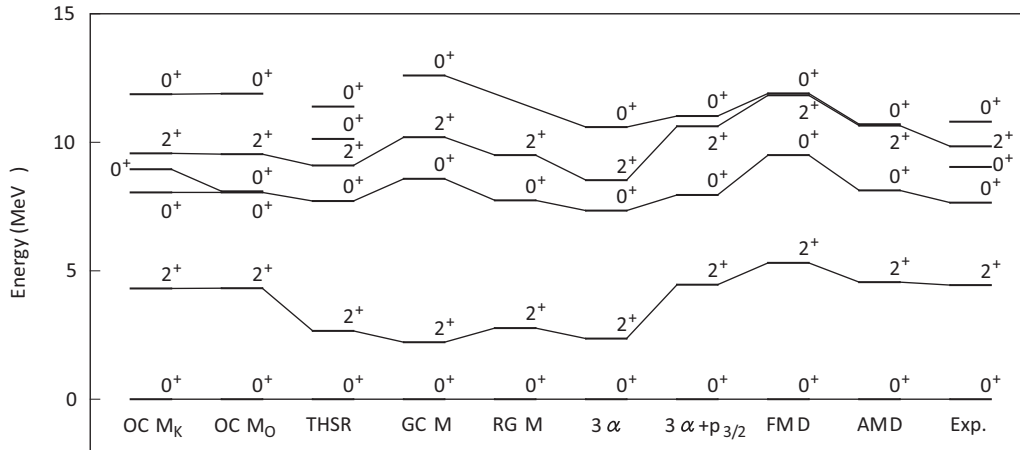
FIG. 7. Comparison of levels from a semimicroscopic 3α-cluster model (OCM$_K$ [27,28] and OCM$_O$ [29]), microscopic 3α-cluster models (THSR [15], GCM [9], RGM [10], and 3α), and models including α-cluster breaking component ($3\alpha + p_{3/2}$, FMD [6], and AMD [5]) with experimental data [25,36].

We comment on the dependence on the width parameter of the $p_{3/2}$ subshell closure wave function. In the present study, we adopted the same width parameter of the $p_{3/2}$ subshell closure wave function with the BB wave functions. In the previous study of ^{12}C with the method of variation after the spin-parity projection in the framework of AMD [5], very similar results to the present ones were obtained even though a different width parameter $\nu = 0.19$ fm^{-2}, which gives a larger radius for $p_{3/2}$ subshell closure wave function, was adopted. Therefore, we expect the results are not so sensitive to the choice of the width parameter, and even if we choose the different width parameter from the present study, we will obtain qualitatively similar results. The further investigation using the different width parameters between the $p_{3/2}$ subshell closure wave function and BB wave functions is a future problem.

B. Comparison with other models

In Fig. 7, we compare energy levels obtained from the 3α and $3\alpha + p_{3/2}$ calculations of the present results with those from various theoretical models. The first and second columns are the levels calculated by OCM [27–29], which is a semimicroscopic 3α-cluster model. The third, fourth, and fifth columns are those calculated by the microscopic cluster models of THSR [15], GCM [9], and resonating group method (RGM) [10], respectively. In the sixth and seventh columns, the present results for $u_{ls} = 0$ MeV (3α) and $u_{ls} = 1600$ MeV ($3\alpha + p_{3/2}$) for the microscopic calculations without and with α-cluster breaking are shown, respectively. The eighth and ninth columns are the levels calculated by FMD [6] and AMD [5], which are microscopic 12-body approaches without assuming the presence of any cluster and can contain α-cluster breaking components. The tenth column is experimental data [25,36].

The microscopic α-cluster models underestimate the level spacing between the 0_1^+ and 2_1^+ states by about a factor of 2, whereas models that include an α-cluster breaking component reproduce it properly. This is an evidence for α-cluster breaking. The OCM calculations fit this level spacing by hand adjustment of a phenomenological 3α potential.

Experimentally, four 0^+ states have been reported. A newly measured 0^+ state around 10 MeV is missing from theoretical calculations except for the OCM and THSR calculations. Even though the number of 0^+ states obtained in the OCM and THSR calculations is consistent with the experimental result, the calculated energy spectra for the $0_{2,3,4}^+$ and 2_2^+ states around 10 MeV are not satisfactory. The relative energy position of the 2_2^+ state to the 0^+ states is very important for determining the band structure. It is important to reproduce the experimental energy spectra for 0^+ and 2^+ states, including the new 0^+ state, to clarify the structures of excited states near the threshold energy.

In Table V, we compare $E2$ transition strengths from the present results with those from several theoretical models. The labels in the table are the same as those in Fig. 7. The microscopic α-cluster models without α-cluster breaking tend to overestimate the $2_1^+ \rightarrow 0_1^+$ transition strengths, whereas models with α-cluster breaking reproduce it properly. For the reproduction of the $2_2^+ \rightarrow 0_1^+$ transition strength, the present $3\alpha + p_{3/2}$ agrees with the experimental data better than the other models.

The $E2$ transition strengths from the 2_2^+ state are important for determining the band assignment for this state, as discussed before. Although the 2_2^+ state has strong $E2$ transitions to the 0_2^+ and 0_3^+ states, the major transition differs between calculations with and without α-cluster breaking. The $2_2^+ \rightarrow 0_3^+$ transition strength is significantly larger than the $2_2^+ \rightarrow 0_2^+$ one in the $3\alpha + p_{3/2}$ and AMD calculations with α-cluster breaking. However, the relation of strengths is opposite and the $2_2^+ \rightarrow 0_2^+$ transition is dominant in the 3α and THSR calculations without α-cluster breaking. This implies that the bandhead of the 2_2^+ state is changed from the 0_2^+ state to the 0_3^+ state by α-cluster breaking. This difference between calculations with and without α-cluster breaking comes from the difference of cluster configurations in the 0_2^+ and 0_3^+ states due to α-cluster breaking. As explained above, with α-cluster breaking, the cluster development of the 0_2^+ state is reduced to decrease the $E2$ transition from the 2_2^+ state. Moreover, the structure of the 0_3^+ state changes from the

TABLE V. Comparison of $E2$ transition strengths between 0^+ and 2^+ states. Labels are the same as in Fig. 7. The unit is e^2 fm^4.

	Model							
Transition	THSR	GCM	RGM	3α	$3\alpha + p_{3/2}$	FMD	AMD	Expt.
$2_1^+ \to 0_1^+$	9.5	8.0	9.3	10.8	7.4	8.69	8.5	7.6 ± 0.4
$2_1^+ \to 0_2^+$	0.97	0.7	1.1	1.4	5.1	3.83	5.1	2.6 ± 0.4
$2_1^+ \to 0_3^+$				0.4	0.2			
$2_2^+ \to 0_1^+$	2.4		2.5	4.0	1.1		0.4	$1.57^{+0.14}_{-0.11}$
$2_2^+ \to 0_2^+$	295		210	183	76.5		102	
$2_2^+ \to 0_3^+$	104			64.4	166		311	

vibration mode of acute and obtuse triangle configurations of three α clusters to a chainlike open triangle structure. Therefore, the phase with the 2_2^+ becomes more coherent in the results with α-cluster breaking. We stress that α-cluster breaking caused by the spin-orbit force has significant effects on transition strengths and changes band structure. This implies that, to investigate structures of excited cluster states in ^{12}C, it is important to consider α-cluster breaking, in particular, mixing of the $p_{3/2}$ subshell closure configuration in 0^+ states.

C. Linear chainlike band

In the results with α-cluster breaking, we assigned the 0_3^+ and 2_2^+ states as the band members because of the major $E2$ transition as discussed above. Since the results with α-cluster breaking reproduce the experimental data such as the large level spacing between 0_1^+ and 2_1^+ states, rms radii, and $E2$ transition strengths between low-lying states well, we consider that the 0_3^+ state is likely to be the bandhead of the 2_2^+, although there is no experimental data for the $E2$ transitions from the 2_2^+ state to the 0_2^+ state and the 0_3^+ state.

Strictly speaking, the structure of the 2_2^+ state is different from that of the 0_3^+ state because of 16% of the α-cluster breaking component in the 0_3^+ state (see Table I). It means that they are not an ideal rotational band constructed from an intrinsic state. However, when we project the structures on the 3α-cluster configuration space, we found that both of 0_3^+ and 2_2^+ states have maximum amplitude around obtuse triangle region. Considering these points, the stronger $E2$ transition strength and maximum amplitude around the chainlike open triangle structure, this band can be considered a linear chainlike band.

In this band, the energy position of the 0_3^+ state is slightly higher than that of the 2_2^+ state in the present calculation with α-cluster breaking. The order of the 0^+ state and the 2^+ state is reverse to an ordinary rotational band. This may come from the mixing of the intrinsic structure of the 0_2^+ state in the 2_2^+ state, though the dominant component of the 2_2^+ state is the intrinsic structure of the 0_3^+ state. This can be understood from that the $E2$ transition from the 2_2^+ state is not weak to the 0_2^+ state though the strength is relatively smaller than that to the 0_3^+ state.

V. SUMMARY

To clarify α-cluster breaking effects on 3α-cluster structures in ^{12}C, we investigated ^{12}C with a hybrid model

composed of the BB cluster model and the $p_{3/2}$ subshell closure wave function. We superposed 252 BB wave functions to sufficiently describe the relative motions of clusters. The α-cluster breaking caused by the spin-orbit force affects 0^+ states through the mixing of the $p_{3/2}$ subshell closure wave function. The present result reproduces well the experimental results with the significant mixing of α-cluster breaking. We have found that α-cluster breaking significantly changes the cluster structures of 0^+ states through orthogonality to lower states. As a result of the structure changes of 0^+ states, the band assignment for the 2_2^+ state is changed. To investigate α-cluster breaking effects, we compared 3α configurations contained in 0^+ states obtained from calculations with and without α-cluster breaking.

In calculations with and without α-cluster breaking, the 0_1^+ state has a compact 3α-cluster structure as the dominant component and also contains components of developed cluster configurations. However, in the calculation with α-cluster breaking, 3α-cluster components becomes relatively small because of significant mixing of the $p_{3/2}$ subshell closure component.

In both calculations, the 0_2^+ state is described by the superposition of various triangle configurations of three α clusters. However, in the calculation with α-cluster breaking, the spatial development of the cluster structure and the gaslike feature of the 0_2^+ state are slightly reduced. Orthogonality to the 0_1^+ state cannot hinder the 0_2^+ state including more compact α-cluster components because the 3α-cluster component in the 0_1^+ state decreases with α-cluster breaking.

Because of α-cluster breaking, the structure of the 0_3^+ state changes from the vibration mode of acute and obtuse triangle configurations to the chainlike open triangle structure. The components of acute triangle configurations increases in the 0_2^+ state; therefore, the 0_3^+ state loses components of acute triangle configurations because of orthogonality to the 0_2^+ state.

Because of structure changes of 0^+ states by α-cluster breaking, transition strengths change significantly. The band assignment for the 2_2^+ state differs between calculations with and without α-cluster breaking. Namely, in the model calculation without α-cluster breaking, the 0_2^+ state is assigned to be the bandhead of the 2_2^+ state. However, when we incorporate α-cluster breaking caused by the spin-orbit force, the 0_3^+ state is regarded as the bandhead of the 2_2^+ state. The 0_3^+ state is

likely to be the bandhead of the $2_2{}^+$ state instead of the $0_2{}^+$ state because the present calculation reproduces experimental data of the low-lying states well with α-cluster breaking. Considering the stronger $E2$ transition strength and maximum amplitude around the chainlike open triangle structure, this band can be considered a linear chainlike band. Unfortunately, there are no experimental data for the $E2$ transitions from the $2_2{}^+$ state to excited 0^+ states. Moreover, experimental information about two 0^+ states around 10 MeV is not enough to assign the theoretical $0_3{}^+$ state to either of the experimental 0^+ states. Further experimental data related to 0^+ and 2^+ states in this energy region are required to clarify the band assignment of these states.

We stress that α-cluster breaking caused by the spin-orbit force gives significant effect on cluster structures, transition strengths, and band structure. To investigate structures of excited cluster states in ^{12}C, it is important to consider α-cluster breaking, in particular, mixing of the $p_{3/2}$ subshell closure configuration in 0^+ states.

[1] K. Ikeda, N. Takigawa, and H. Horiuchi, Prog. Theor. Phys. Suppl. **E68**, 464 (1968).

[2] N. Itagaki, S. Aoyama, S. Okabe, and K. Ikeda, Phys. Rev. C **70**, 054307 (2004).

[3] Y. Kanada-En'yo, Phys. Rev. Lett. **81**, 5291 (1998).

[4] T. Neff and H. Feldmeier, Nucl. Phys. A **738**, 357 (2004).

[5] Y. Kanada-En'yo, Prog. Theor. Phys. **117**, 655 (2007).

[6] M. Chernykh, H. Feldmeier, T. Neff, P. von Neumann-Cosel, and A. Richter, Phys. Rev. Lett. **98**, 032501 (2007).

[7] Y. Kanada-En'yo, M. Kimura, and A. Ono, Prog. Theor. Exp. Phys. **2012**, 01A202 (2012).

[8] Y. Fukuoka, S. Shinohara, Y. Funaki, T. Nakatsukasa, and K. Yabana, Phys. Rev. C **88**, 014321 (2013).

[9] E. Uegaki, S. Okabe, Y. Abe, and H. Tanaka, Prog. Theor. Phys. **57**, 1262 (1977).

[10] Y. Fukushima and M. Kamimura, in *Proceedings of the International Conference on Nuclear Structure, Tokyo, 1977*, edited by T. Marumori [J. Phys. Soc. Jpn. **44**, 225 (1978)].

[11] A. Tohsaki, H. Horiuchi, P. Schuck, and G. Röpke, Phys. Rev. Lett. **87**, 192501 (2001).

[12] Y. Funaki, A. Tohsaki, H. Horiuchi, P. Schuck, and G. Röpke, Phys. Rev. C **67**, 051306(R) (2003).

[13] Y. Funaki, A. Tohsaki, H. Horiuchi, P. Schuck, and G. Röpke, Eur. Phys. J. A **24**, 321 (2005).

[14] T. Suhara, Y. Funaki, B. Zhou, H. Horiuchi, and A. Tohsaki, Phys. Rev. Lett. **112**, 062501 (2014).

[15] Y. Funaki, arXiv:1408.5855; (private communication).

[16] T. Yamada, Y. Funaki, H. Horiuchi, K. Ikeda, and A. Tohsaki, Prog. Theor. Phys. **120**, 1139 (2008).

[17] P. Navrátil and W. E. Ormand, Phys. Rev. C **68**, 034305 (2003).

[18] P. Navrátil, S. Quaglioni, I. Stetcu, and B. R. Barrett, J. Phys. G: Nucl. Part. Phys. **36**, 083101 (2009).

[19] T. Neff and H. Feldmeier, J. Phys. Conf. Ser. **111**, 012007 (2008).

[20] E. Epelbaum, H. Krebs, T. A. Lähde, D. Lee, and U. G. Meißner, Phys. Rev. Lett. **109**, 252501 (2012).

[21] T. Suhara and Y. Kanada-En'yo, Prog. Theor. Phys. **123**, 303 (2010).

[22] M. Freer, H. Fujita, Z. Buthelezi, J. Carter, R. W. Fearick, S. V. Fortsch, R. Neveling, S. M. Perez, P. Papka, F. D. Smit, J. A. Swartz, and I. Usman, Phys. Rev. C **80**, 041303(R) (2009).

[23] M. Itoh *et al.*, Phys. Rev. C **84**, 054308 (2011).

[24] W. R. Zimmerman *et al.*, Phys. Rev. Lett. **110**, 152502 (2013).

[25] W. R. Zimmerman, Ph.D. dissertation, University of Connecticut, 2013.

[26] M. Itoh *et al.*, J. Phys. Conf. Ser. **436**, 012006 (2013).

[27] C. Kurokawa and K. Katō, Phys. Rev. C **71**, 021301 (2005).

[28] C. Kurokawa and K. Katō, Nucl. Phys. A **792**, 87 (2007).

[29] S. Ohtsubo, Y. Fukushima, M. Kamimura, and E. Hiyama, Prog. Theor. Exp. Phys. **2013**, 073D02 (2013).

[30] D. M. Brink, in *Proceedings of the International School of Physics Enrico Fermi, Course 36, Varenna*, edited by C. Bloch (Academic, New York, 1966).

[31] S. Okabe and Y. Abe, Prog. Theor. Phys. **61**, 1049 (1979).

[32] N. Itagaki, H. Masui, M. Ito, and S. Aoyama, Phys. Rev. C **71**, 064307 (2005).

[33] T. Suhara, N. Itagaki, J. Cseh, and M. Płoszajczak, Phys. Rev. C **87**, 054334 (2013).

[34] A. Volkov, Nucl. Phys. **74**, 33 (1965).

[35] N. Yamaguchi, T. Kasahara, S. Nagata, and Y. Akaishi, Prog. Theor. Phys. **62**, 1018 (1979).

[36] F. Ajzenberg-Selove and J. H. Kelley, Nucl. Phys. A **506**, 1 (1990).

[37] A. Ozawa, T. Suzuki, and I. Tanihata, Nucl. Phys. A **693**, 32 (2001).

[38] A. N. Danilov, T. L. Belyaeva, A. S. Demyanova, S. A. Goncharov, and A. A. Ogloblin, Phys. Rev. C **80**, 054603 (2009).